LETTERS

Seismic detection of folded, subducted lithosphere at the core–mantle boundary

Alexander R. Hutko[1], Thorne Lay[1], Edward J. Garnero[2] & Justin Revenaugh[3]

Seismic tomography has been used to infer that some descending slabs of oceanic lithosphere plunge deep into the Earth's lower mantle[1,2]. The fate of these slabs has remained unresolved, but it has been postulated that their ultimate destination is the lowermost few hundred kilometres of the mantle, known as the D″ region. Relatively cold slab material may account for high seismic velocities imaged in D″ beneath areas of long-lived plate subduction, and for reflections from a seismic velocity discontinuity just above the anomalously high wave speed regions[3,4]. The D″ discontinuity itself is probably the result of a phase change in relatively low-temperature magnesium silicate perovskite[5,6]. Here, we present images of the D″ region beneath the Cocos plate using Kirchhoff migration of horizontally polarized shear waves, and find a 100-km vertical step occurring over less than 100 km laterally in an otherwise flat D″ shear velocity discontinuity. Folding and piling of a cold slab that has reached the core–mantle boundary, as observed in numerical and experimental models, can account for the step by a 100-km elevation of the post-perovskite phase boundary due to a 700 °C lateral temperature reduction in the folded slab. We detect localized low velocities at the edge of the slab material, which may result from upwellings caused by the slab laterally displacing a thin hot thermal boundary layer.

The Earth's D″ region contains a large thermal boundary layer caused by heat flowing from the molten iron-alloy outer core into the crystalline silicate/oxide mantle. However, a thermal boundary alone cannot account for all seismically detected structures in D″ (ref. 3), such as an abrupt increase in seismic velocities detected at heights varying from 130 to 340 km above the core–mantle boundary (CMB). Shear (S) and compressional (P) wave velocity increases at this D″ discontinuity range from 1–3% and 0.5–3%, respectively, and vary spatially. A recently discovered phase transition in $(Mg,Fe)SiO_3$ perovskite is predicted to occur at pressures and temperatures near the top of the D″ region, offering a viable explanation for the D″ discontinuity[5,6]. It is important to assess whether thermal and phase-change effects can account for the discontinuity, or whether additional chemical heterogeneity is required[3,7–9].

P and S wave global tomography studies indicate an anomalously fast quasi-tabular structure extending deep into the lower mantle beneath the Caribbean[1,2], attributed to the thermal effect of remnant Farallon slab, which is comprised of former eastern Pacific basin oceanic lithosphere. If this material reaches the CMB, it should elevate the velocity discontinuity owing to the large positive Clapeyron slope of the perovskite/post-perovskite phase transition[10]. Seismological investigations of the D″ region below the localized region under the Cocos plate have found small-scale variations in D″ velocity structure using S and P waves[11,12], apparent topography of a pervasive D″ shear velocity reflector[13,14], and apparent anisotropy in D″ (ref. 15).

Given the uncertain fate of slab material, we employ an imaging approach that makes minimal assumptions about the geometry of structures that give rise to seismic wave arrivals, Kirchhoff migration, or diffraction-stacking, which allows seismic waves to originate anywhere within a three-dimensional volume. This method is ideal for imaging unknown deep mantle slab configurations[13,16–19], discontinuities with strong topography or limited lateral extent, and localized heterogeneities such as plumes rising from the CMB. We apply Kirchhoff migration to a data set previously processed for one-dimensional stacking[11] to determine the lowermost-mantle shear velocity structure beneath the Cocos Plate (Fig. 1). The data have stable horizontal shear (SH) radiation of S and core-reflected ScS waves, and are processed to obtain dominant periods of about 3 s.

Our Kirchhoff approach[17] assumes isotropic single-scattering: when an incident SH wave encounters a point scatterer, a scattered

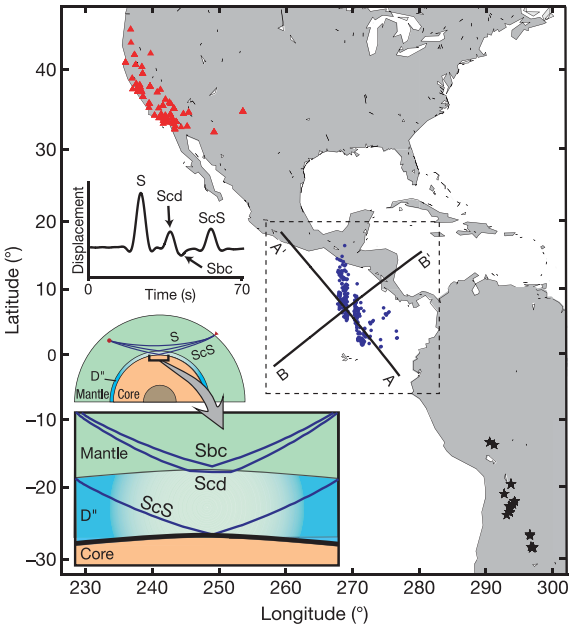

Figure 1 | Map showing earthquake epicentres (black stars), seismic station locations (red triangles) and ScS reflection points (blue dots). Also shown are the two lines along which cross-sections are made through the migration image volume in the lower mantle (black lines). The bottom left inset shows S and ScS raypaths through the mantle. At long epicentral distances, the direct S wave turns deep in the lowermost mantle and the phases interacting with the D″ discontinuity have their largest amplitudes. A representative synthetic seismogram is shown, illustrating the small negative overshoot of the Scd + Sbc arrival between S and ScS arrivals.

[1]Earth Sciences Department, University of California Santa Cruz, 1156 High Street, Santa Cruz, California 95064, USA. [2]Department of Geological Sciences, Arizona State University, Box 871404, Tempe, Arizona 85287-1404, USA. [3]Department of Geology and Geophysics, University of Minnesota, 310 Pillsbury Dr. SE, Minneapolis, Minnesota 55455, USA.

signal propagates to receivers without further interaction with other scatterers. This is valid for velocity heterogeneity strengths less than a few per cent. The travel times from every source and receiver are calculated to possible scattering locations within a three-dimensional grid emplaced in the lower mantle. The differential time between a given scattering location arrival and either S or ScS is computed for time-shifting each seismogram relative to the reference phase. Shifted seismograms for all source–receiver combinations are linearly summed to obtain an estimate of the wave amplitude associated with each candidate scattering location. We only consider energy that is scattered with upward-directed raypaths to the source and receiver, which excludes possible polarity reversals caused by underside reflections or scattering.

Vertical cross-sections (Fig. 2) through the data migration volume show strong reflectance associated with the CMB and the D″ discontinuity. The CMB is illuminated by ScS, and as expected, imaged as an extensive, nearly horizontal scattering surface. The D″ discontinuity is illuminated by large positive-amplitude post-critical refracted phases (called Scd, ref. 20), and small negative-amplitude phase-shifted post-critical reflected phases (Sbc, see Fig. 1). The D″ discontinuity is 160–190 km above the CMB towards the southeast, and 250–290 km above the CMB in the northwest of our study region. We note that migrations directly depend on the assumed reference model: the discontinuity depth maps 50–100 km deeper using the PREM[21] reference model than it does for migrations using models with higher velocities in D″. The apparent D″ discontinuity depth differs by up to 70 km depending on whether S or ScS is the reference phase. However, the abrupt step is unequivocally present in all cases and the step amplitude changes by less than 20 km. This stability adds confidence that the step is not an artefact of earthquake mislocation or localized regions of velocity heterogeneity sampled by the reference phase. Kirchhoff migration theory assumes pre-critical reflections and does not account for wavefield triplication effects from a velocity discontinuity within the image volume; it thus slightly underestimates depth and blurs the image of the reflector because the higher-amplitude, refracted Scd phase turns below the discontinuity, arriving slightly before reflected energy. Even so, these are the highest-resolution three-dimensional deep-mantle reflector images of the lower mantle so far, adding refined focus to past work that infers a larger sloping discontinuity gradient in this region[13].

To address the trade-off between discontinuity depth and volumetric heterogeneity we compute travel-time perturbations through mantle tomography models (UT[2], UCB[22], CIT[23]) for the unperturbed raypaths of both reference phases and the scattering raypath geometries (Fig. 3). Images for different tomography models suggest lateral disruption of the discontinuity near 6° N, and vertical offsets across

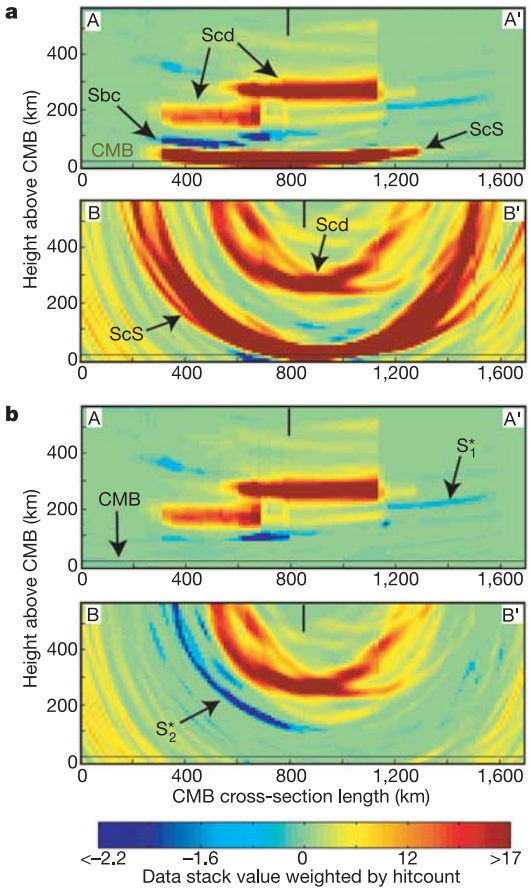

Figure 2 | Vertical cross-sections through the scattering image volume for our data set migrated in the PREM model using ScS as the reference phase. The horizontal axis in each panel is lateral distance going from A–A′ and B–B′ spanning approximately 1,700 km. The black tick mark indicates where the two profiles cross each other. The D″ discontinuity can be seen in **a** along A–A′ at about 180 and 280 km above the CMB in the southeast and northwest parts of the image, respectively. The images in **b** are the same as in **a** except that the ScS energy has been censored by 4-s-wide tapers. All data stack values (the sum of seismogram amplitudes aligned along travel times corresponding to a scattered phase originating from a given grid point) have been weighted according to the hitcount (the number of contributing seismograms). There is no vertical exaggeration.

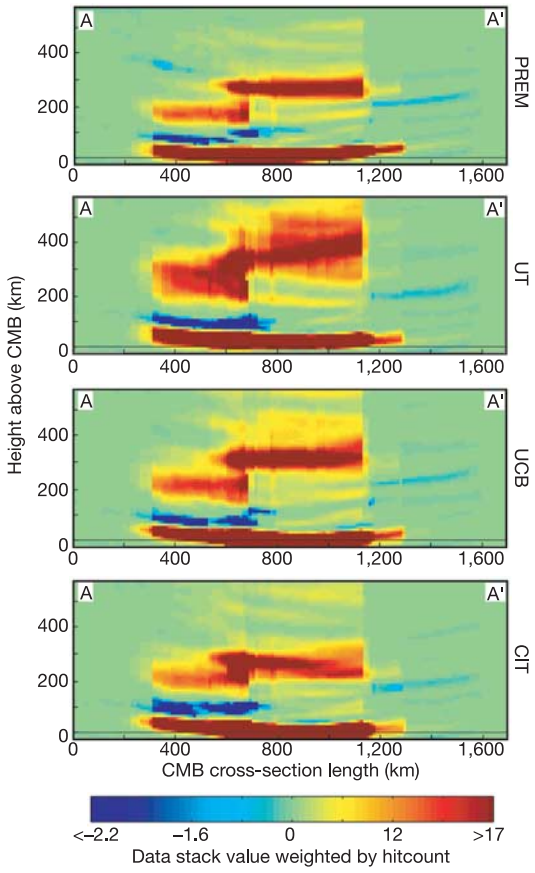

Figure 3 | Vertical cross-sections along profile A-A′ through the image volume migrated relative to ScS using four different velocity models. Models are identified on the right axis. The direct S wave energy has been suppressed by 4-s-wide tapers. Data stack values have been weighted according to the hitcount. Profiles are chosen along the ray-path corridor (A–A′), because oblique profiles through the image volume will blend together the well-resolved in-plane images with more poorly resolved out-of-plane images, which have much more streaking.

the discontinuity step of 50 to 150 km. The discontinuity feature imaged using the UT model is spread out vertically and located at shallower depth than for the PREM migrations. These effects stem from relatively high lowermost-mantle shear velocities of the UT model. This should not be construed as a deterioration of the images relative to those found using PREM; lower reference velocities intrinsically sharpen reflector images. The CIT model, which has a northward decrease in velocity in the D″ layer, tends to suppress the vertical offset by about 50 km, but does not eliminate it. However, this model does not predict a northward decrease of ScS–S differential times, as is clearly observed in the data. ScS–S differential time predictions from the UT and UCB models are consistent with the data; the UT and UCB models increase the imaged discontinuity step height relative to the PREM-derived image by about 10 km.

Our migrations cannot preclude the existence of small-scale (<30 km vertically) undulations in the reflecting surface. However, images for all reference models (Fig. 3) are compatible with a quasi-horizontal reflector over a horizontal scale of 800 km offset by a step in the discontinuity depth. The multiple-event stacking here strongly favours an abrupt feature (occurring over less than 100 km laterally) rather than the smooth feature inferred in ref. 13 which averaged highly dispersed reflector images from small subsets of data for individual events.

Cross-sections through the scattering volume also show weak negative amplitude (blue) features with significant coherence. A fairly narrow blue streak appears below the discontinuity (red) in the southeast. This feature is concentrated in the plane of propagation and is a predictable artefact of the phase-shifted post-critical reflection associated with the overlying discontinuity, as confirmed by migrating synthetic seismograms. A small negative-amplitude feature (S_1^*) also extends northwestward from the northern end of the positive reflector at a height of about 220 km above the CMB. This feature is faint because only data from the two northernmost earthquakes adequately sample it. The image is consistent with streaking from a low-velocity point-scatterer on the margin of the illuminated zone. This feature is not present in the three global tomography models; however, a recent finite frequency regional tomography model[24] shows evidence for it. Other faint positive- and negative-amplitude features (Fig. 2), especially shallow ones, may be crustal multiples that persist due to incomplete suppression of receiver coda following the direct S wave.

A prominent negative-amplitude feature (S_2^*) is present in migration volume cross-sections perpendicular to the raypaths when ScS arrivals are muted out (Fig. 2b). These cross-sections display the classic 'smiles' of scattering migrations that appear when the data sample only a limited azimuthal corridor, as in our case. Although the location is not well resolved, the negative-amplitude feature is strongest at a height of about 200 km above the CMB, on the southwest edge of the northwestern, shallower positive discontinuity (see Supplementary Information for more cross-sections). Using a migration approach with smaller data sets, a prior study implied that a negative reflector exists below the positive reflector in the northwest[13]. Our results show very little coherent negative in-plane energy at depths below the D″ discontinuity towards the northwest, which is consistent with results from one-dimensional waveform stacking[11]; however, all of our models indicate that a negative-amplitude scatterer is offset to the southwest. Out-of-plane scattering produces an arrival, readily apparent in waveforms from central California stations[13] that approaches the ScS arrival and does not stack coherently for in-plane sections or one-dimensional stacks (see Supplementary Information).

The cause of the D″ discontinuity remains uncertain[3]. There is currently much enthusiasm for interpreting the P and S velocity discontinuities near the top of D″ as the result of the $(Mg,Fe)SiO_3$ perovskite to post-perovskite phase transformation[5,6]. This phase change is predicted to have a large positive Clapeyron slope of about 7.5 MPa K^{-1} (ref. 10). To account for a 100-km step in the D″ discontinuity by purely thermal effects, a lateral temperature gradient of 700 K is required over less than ~100 km laterally. Such a large lateral temperature gradient clearly requires a dynamic environment. Recent geodynamic calculations[25] indicate that slabs descending to the base of the mantle can retain strong lateral temperature gradients and buckle and spread out as they approach the CMB. Folding of the Farallon slab and spreading to the west offers a viable explanation for the strong lateral temperature gradients that interact with the phase-change sensitivity to produce the observed step in the D″ discontinuity (Fig. 4).

A recent study proposed a vertical pairing of overlying positive and negative velocity discontinuities due to transformation to post-perovskite at the top of D″ and then back to perovskite in a high-temperature gradient at greater depth[26], but there is no indication of a second, deeper horizontal velocity discontinuity in our migrations. Forward modelling with reflectivity synthetics establishes that a reflected phase from a horizontal discontinuity with a 5–10% shear velocity decrease is needed to produce reflections large enough to be observed in individual traces (see Supplementary Information). Thus any second phase-transformation feature is predicted[27] to be below the noise level of these and earlier[13] migration images. Some strong negative-amplitude arrivals are apparent in the individual waveforms but these have travel times suggesting an out-of-plane scattering origin. Focusing by a three-dimensional low-velocity structure can produce comparable arrivals with a less pronounced velocity decrease. Lacking constraints on the scattering geometry, we cannot fully quantify the velocity anomaly involved, but an irregular structure with 3–10% low velocities and optimal focusing could account for the observed arrivals.

These three-dimensional low-velocity features at the edges of the shallower discontinuity image may be associated with lateral gradients in temperature on the margin of slab material and a resulting semi-vertical boundary to the phase change. Both features are imaged by scattered arrivals that arrive before and after ScS: such phases will not strongly illuminate a near-horizontal reflector, so this

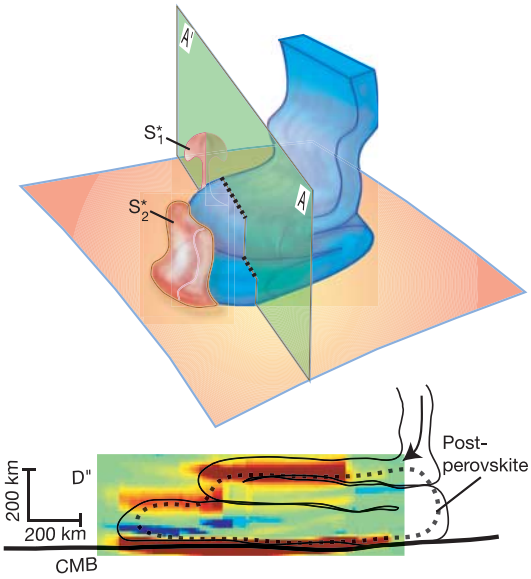

Figure 4 | A cold buckled subducted slab (blue) in the lowermost mantle may account for the thermal structure that results in a step in the perovskite/post-perovskite phase transition. Low-velocity scattering structures (S_1^*, S_2^*) on the lateral margins of the slab pile are postulated to account for the concentrated scatterers that are imaged. The green plane represents the profile A–A′ through the migration volume used in Figs 1–3. The image in the lower panel is taken from profile A–A′ in Fig. 2a, with positive-amplitude reflectivity (red) and negative-amplitude reflectivity (blue).

is likely to involve concentrated volumetric scatterers. Because any lateral velocity gradients from thermal and phase change effects are going to involve a reduction in velocity of only a few per cent, an additional contribution is needed to concentrate the heterogeneity. One viable candidate is small boundary-layer instabilities or plumes caused by slab material descending upon the CMB, extruding the hot basal layer of the thermal boundary layer, and prompting upwelling instabilities[25] of partial melt with strong velocity reductions. A lateral gradient of composition, perhaps of iron or aluminium content, could augment any thermal effects on the depth of the phase boundary[6]. However, for isolated chemical compositions to maintain such a steep slope, a very active process must be present to sustain it.

Our image volume is constrained by the path coverage, but the method could expand to cover a larger volume as more source/station geometries are included. The large step in the D″ reflector is comparable to features in continental lithosphere, which involve long-term thermal and chemical contrasts.

Received 23 December 2005; accepted 22 March 2006.

1. Grand, S. P., van der Hilst, R. D. & Widiyantoro, S. Global seismic tomography: a snapshot of convection in the Earth. *GSA Today* **7,** 1–7 (1997).
2. Grand, S. P. Mantle shear-wave tomography and the fate of subducted slabs. *Phil. Trans. R. Soc. Lond. A* **360,** 2475–2491 (2002).
3. Lay, T. & Garnero, E. J. in *The State of the Planet: Frontiers and Challenges in Geophysics* (eds Sparks, R. S. J. & Hawkesworth, C. J.) 25–41 (Geophysical Monograph 150, American Geophysical Union, Washington DC, 2004).
4. Wysession, M. E., *et al.* in *The Core-Mantle Boundary Region* (eds Gurnis, M., Wysession, M. E., Knittle, E. & Buffett, B. A.) 273–298 (Geodynamics Series 28, American Geophysical Union, Washington DC, 1998).
5. Murakami, M., Hirose, K., Kawamura, K., Sata, N. & Ohishi, Y. Post-perovskite phase transition in $MgSiO_3$. *Science* **304,** 855–858 (2004).
6. Lay, T. *et al.* Multidisciplinary impact of the deep mantle phase transition in perovskite structure. *Eos* **86,** 1, 5 (2005).
7. Masters, G., Laske, G., Bolton, H. & Dziewonski, A. M. in *Earth's Deep Interior: Mineral Physics and Tomography from the Atomic to the Global Scale*, (eds Karato, S., Forte, A. M., Liebermann, R. C., Masters, G. & Stixrude, L.) 63–87 (American Geophysical Union, Washington DC, 2000).
8. Wen, L., Silver, P., James, D. & Kuehnel, R. Seismic evidence for a thermo-chemical boundary at the base of the Earth's mantle. *Earth Planet. Sci. Lett.* **189,** 141–153 (2001).
9. Ni, S. & Helmberger, D. V. Ridge-like lower mantle structure beneath South Africa. *J. Geophys. Res.* **108,** doi:10.1029/2001JB001545 (2003).
10. Oganov, A. R. & Ono, S. Theoretical and experimental evidence for a post-perovskite phase of $MgSiO_3$ in Earth's D″ layer. *Nature* **430,** 445–448 (2004).
11. Lay, T., Garnero, E. J. & Russell, S. A. Lateral variation of the D″ discontinuity beneath the Cocos Plate. *Geophys. Res. Lett.* **31,** doi: 10.1029/2004GL020300 (2004).
12. Reasoner, C. & Revenaugh, J. Short-period P wave constraints on D″ reflectivity. *J. Geophys. Res.* **104,** 955–961 (1999).
13. Thomas, C., Garnero, E. J. & Lay, T. High-resolution imaging of lowermost mantle structure under the Cocos Plate. *J. Geophys. Res.* **109,** doi: 10.1029/2004JB003013 (2004).
14. Ding, X. & Helmberger, D. V. Modeling D″ structure beneath Central America with broadband seismic data. *Phys. Earth Planet. Inter.* **101,** 245–270 (1997).
15. Rokosky, J. M., Lay, T., Garnero, E. J. & Russell, S. A. High-resolution investigation of shear wave anisotropy in D″ beneath the Cocos Plate. *Geophys. Res. Lett.* **31,** L07605, doi: 10.1029/2003GL018902 (2004).
16. Lay, T. & Young, C. J. Imaging scattering structures in the lower mantle by migration of long-period S waves. *J. Geophys. Res.* **101,** 20023–20040 (1996).
17. Revenaugh, J. A scattered-wave image of subduction beneath the Transverse Ranges, California. *Science* **268,** 1888–1892 (1995).
18. Thomas, C., Weber, M., Wicks, C. W. & Scherbaum, F. Small scatterers in the lower mantle observed at German broadband arrays. *J. Geophys. Res.* **104,** 15073–15088 (1999).
19. Kito, T., Krüger, F. & Negishi, H. Seismic heterogeneous structure in the lowermost mantle beneath the southwestern Pacific. *J. Geophys. Res.* **109,** B09304, doi: 10.1029/2003JB002677 (2004).
20. Lay, T. & Helmberger, D. V. A lower mantle S-wave triplication and the shear velocity structure of D. *Geophys. J. R. Astron. Soc.* **75,** 799–837 (1983).
21. Dziewonski, A. M. & Anderson, D. L. Preliminary reference Earth model. *Phys. Earth Planet. Inter.* **25,** 297–356 (1981).
22. Megnin, C. & Romanowicz, B. The three-dimensional shear velocity structure of the mantle from the joint inversion of body, surface, and higher mode waveforms. *Geophys. J. Int.* **143,** 709–728 (2000).
23. Ritsema, J. & Van Heijst, H. J. Seismic imaging of structural heterogeneity in Earth's mantle: evidence for large-scale mantle flow. *Sci. Prog. (New Haven)* **83,** 243–259 (2000).
24. Hung, S.-H., Garnero, E. J., Chiao, L.-Y., Kuo, B.-Y. & Lay, T. Finite-frequency tomography of D″ shear velocity heterogeneity beneath the Caribbean. *J. Geophys. Res.* **110,** B07305, doi: 10.1029/2004JB003373 (2005).
25. Tan, E., Gurnis, M. & Han, L. Slabs in the lower mantle and their modulation of plume formation. *Geochem. Geophys. Geosyst.* **3,** 1067, doi: 10.1029/2001GC000238 (2002).
26. Hernlund, J. W., Thomas, C. & Tackley, P. J. A doubling of the post-perovskite phase boundary and structure of the Earth's lowermost mantle. *Nature* **434,** 882–886 (2005).
27. Flores, C. & Lay, T. The trouble with seeing double. *Geophys. Res. Lett.* **32,** L24305, doi: 10.1029/2005GL024366 (2005).

Supplementary Information is linked to the online version of the paper at www.nature.com/nature.

Acknowledgements M. Thorne provided three-dimensional finite difference synthetics for versions of our step discontinuity structure. We also thank Q. Williams for discussions.

Author Information Reprints and permissions information is available at npg.nature.com/reprintsandpermissions. The authors declare no competing financial interests. Correspondence and requests for materials should be addressed to A.R.H. (ahutko@pmc.ucsc.edu).